Int J Earth Sci (Geol Rundsch)
DOI 10.1007/s00531-013-0873-9

ORIGINAL PAPER

The geometry of the active strike-slip El Tigre Fault, Precordillera of San Juan, Central–Western Argentina: integrating resistivity surveys with structural and geomorphological data

Sabrina Y. Fazzito · José M. Cortés · Augusto E. Rapalini · Carla M. Terrizzano

Received: 12 April 2012 / Accepted: 10 February 2013

Abstract The geometry and related geomorphological features of the right-lateral strike-slip El Tigre Fault, one of the main morphostructural discontinuities in the Central–Western Precordillera of Argentina, were investigated. Achievements of this survey include: recognition of structural and geometrical discontinuities along the fault trace, identification and classification of landforms associated with local transpressional and transtensional sectors, observation of significant changes in the fault strike and detection of right and left bends of different wavelength. In the Central Segment of the El Tigre Fault, 2D electrical resistivity tomography surveys were carried out across the fault zone. The resistivity imaging permitted to infer the orientation of the main fault surface, the presence of blind fault branches along the fault zone, tectonic tilting of the Quaternary sedimentary cover, subsurface structure of pressure ridges and depth to the water table. Based on this information, it is possible to characterize the El Tigre Fault also as an important hydro-geological barrier. Our survey shows that the main fault surface changes along different segments from a high-angle to a subvertical setting whilst the vertical-slip component is either reverse or normal, depending on the local transpressive or transtensive regime induced by major bends along the trace. These local variations are expressed as sections of a few kilometres in length with relatively homogeneous behaviour and frequently separated by oblique or transversal structures.

Keywords El Tigre Fault · Argentine Precordillera · Neotectonics · Fault structure · Geomorphology · 2D electrical resistivity tomography

Electronic supplementary material The online version of this article (doi:10.1007/s00531-013-0873-9) contains supplementary material, which is available to authorized users.

S. Y. Fazzito (✉) · J. M. Cortés · A. E. Rapalini · C. M. Terrizzano
Departamento de Ciencias Geológicas, Facultad de Ciencias Exactas Y Naturales, Instituto de Geociencias Básicas, Aplicadas y Ambientales de Buenos Aires (IGEBA), Universidad de Buenos Aires, Intendente Güiraldes 2160, Pabellón II, Ciudad Universitaria, C1428EGA Buenos Aires, Argentina
e-mail: sabrinafazzito@gl.fcen.uba.ar

J. M. Cortés
e-mail: cortes@gl.fcen.uba.ar

A. E. Rapalini
e-mail: rapalini@gl.fcen.uba.ar

C. M. Terrizzano
e-mail: cterrizzano@gl.fcen.uba.ar

S. Y. Fazzito · J. M. Cortés · A. E. Rapalini · C. M. Terrizzano
Consejo Nacional de Investigaciones Científicas y Técnicas (CONICET), Buenos Aires, Argentina

Introduction

The Andean Precordillera of Argentina, a first-order morphotectonic unit in the Pampean Segment of flat subduction (27°S–33°S), is characterized by a high rate of seismicity and Quaternary tectonic activity (Costa et al. 2006). Along the San Juan and Mendoza Provinces, in fact, the Precordillera corresponds to the seismically most active area of the whole country (INPRES 1977). Hence, identification and characterization of neotectonic structures are of special interest among other objectives to estimate the seismic hazard of the region. In particular, the 120-km-long strike-slip El Tigre Fault (30°12′S–31°14′S, Fig. 1) is regarded as a remarkable feature in the Central–Western Precordillera of the San Juan Province due to its length, quality of exposure and evidence of its Quaternary activity

Published online: 23 March 2013

emphasized by pressure ridges, releasing basins and offset stream channels (INPRES 1982; Bastías et al. 1984; Siame et al. 1997a, b, 2006; Cortés et al. 1999). The actual geometry, extension, kinematics and associated deformational rate of this main fault system have been the subjects of debate. Despite its conspicuous geomorphological character and location in a seismically active region of Argentina, detailed and systematic studies on these features of the El Tigre Fault are very scarce. Very encouraging results have been achieved through the application of geophysical methods for imaging Quaternary structures, such as seismic reflection (Wang 2002; Donne et al. 2007); in this case, however, the use of these methodologies in the study area has just begun (Fazzito et al. 2009; Fazzito 2011). On the other hand, 2D electrical resistivity tomography, a fast and economic method for imaging shallow geological bodies, has been applied with positive conclusions for modelling seismogenic structures along the Precordillera, resulting in better constrains on its geometrical and kinematical properties (Terrizzano et al. 2008, 2010, 2012; Fazzito et al. 2009; Terrizzano 2010; Fazzito 2011).

A structural and geomorphological study along the Central and Southern Segments of the El Tigre Fault together with the results of 8 shallow electrical resistivity models performed in the Central Segment is presented. They contribute to a better characterization of both the subsurface geometry and kinematics of the fault.

Geological frame

At the latitude of the El Tigre Fault, the eastern margin of the Central Andes consists of, from west to east, four first-order morphostructural units: the Frontal Cordillera, the Calingasta–Iglesia Valley, the Precordillera and the Sierras Pampeanas. Between 30°S and 32°S, the Precordillera has been subdivided into three morphotectonic subunits: the Western Precordillera, where the El Tigre Fault is located, the Central and the Eastern Precordillera (Ortiz and Zambrano 1981; Baldis et al. 1982). The Argentine Precordillera is recognized as a fold-and-thrust belt, 400 km long and 80 km wide, uplifted during the Late Cenozoic beginning at around 16 Ma in its northern end and systematically decreasing in age up to 3.5 Ma in its southern tip (Ramos et al. 2002 and references therein). The southern end of the Precordillera coincides with the end of the flat-slab segment (27°S–33°S) of the Central Andes, which has led to interpretations of the uplift of the Argentine Precordillera as closely related with shallowing of the subducted Nazca Plate under South America in the Late Cenozoic (Allmendinger et al. 1990; Kay and Abbruzzi 1996; among others). The Neogene tectonic evolution is characterized by a diachronic migration towards the east of the orogenic front up to the Sierras Pampeanas and the contractional and transpressional deformation of the foreland basin (Isacks and Barazangi 1977; Jordan et al. 1983a, b; Ramos et al. 2002). The Central and Western Precordillera, between 30°S and 31° 30′S in the San Juan Province, constitutes an east-verging thin-skinned belt (Baldis et al. 1982; von Gosen 1995), whilst the Eastern Precordillera is a west verging backthrust system with a deeper level of detachment within the basement, defining a thick skinned triangle zone underneath the Central Precordillera (Zapata and Allmendinger 1996). In the central section of the Precordillera (30°00′S–31°30′S), Quaternary ruptures generally result from the reverse and oblique rejuvenation along segments of range fronts faults. In intermontane basins, folds and fault scarps which affect the piedmont areas are common (Bastías et al. 1990; Cortés et al. 1999; Costa et al. 2000). The eastern flank of the Precordillera, between 31° and 34°S, concentrates most of this active Quaternary deformation (Costa et al. 2006); however, evidence of neotectonic activity has been also reported at the western margin (Cortés and Cegarra 2004; Cortés et al. 2005a, b, c, 2006; Basile 2004; Vallejo 2004; Yamín 2007; Terrizzano 2010). One such example is the displaced Pleistocene sediments along the El Tigre Fault (Bastías and Bastías 1987; Siame et al. 1997b, 2006; Cortés et al. 1999). The Calingasta–Iglesia Valley is a 30-km-wide piggy-back intramontaneous basin (Allmendinger et al. 1990; Beer et al. 1990; Jordan et al. 1993) filled in part with a Miocene–Pliocene volcano-sedimentary succession and Quaternary deposits (Beer et al. 1990) related to different alluvial-fan events and fluvial sediments (Bastías 1985; Siame et al. 1997a).

Stratigraphy

The El Tigre Fault extends approximately between the Jáchal River, to the north, and the San Juan River, to the south (from 30°12′S to 31°14′S, Figs. 1 and 2), in the central region of the Western Precordillera, with a roughly north–south trend (~N7°E). Its southern half cuts the intermountain depression between Sierra del Tigre, to the east, and Sierra de la Crucecita, to the west. On its northern half, the El Tigre Fault becomes more complex with several fault strands on the eastern side of the Iglesia–Calingasta Valley. In this region, the exposed lithostratigraphic units can be grouped into a Palaeozoic–Early Mesozoic substratum constituted by Ordovician marine sedimentary and volcanic rocks (Furque 1963; Cardó and Díaz 2005), Permian marine sequences, Permo–Triassic volcanics and ignimbrites and Late Triassic (Baraldo et al. 1990) continental red beds. On top, some Palaeogene conglomerates and fluvial sandstones underlie the widely

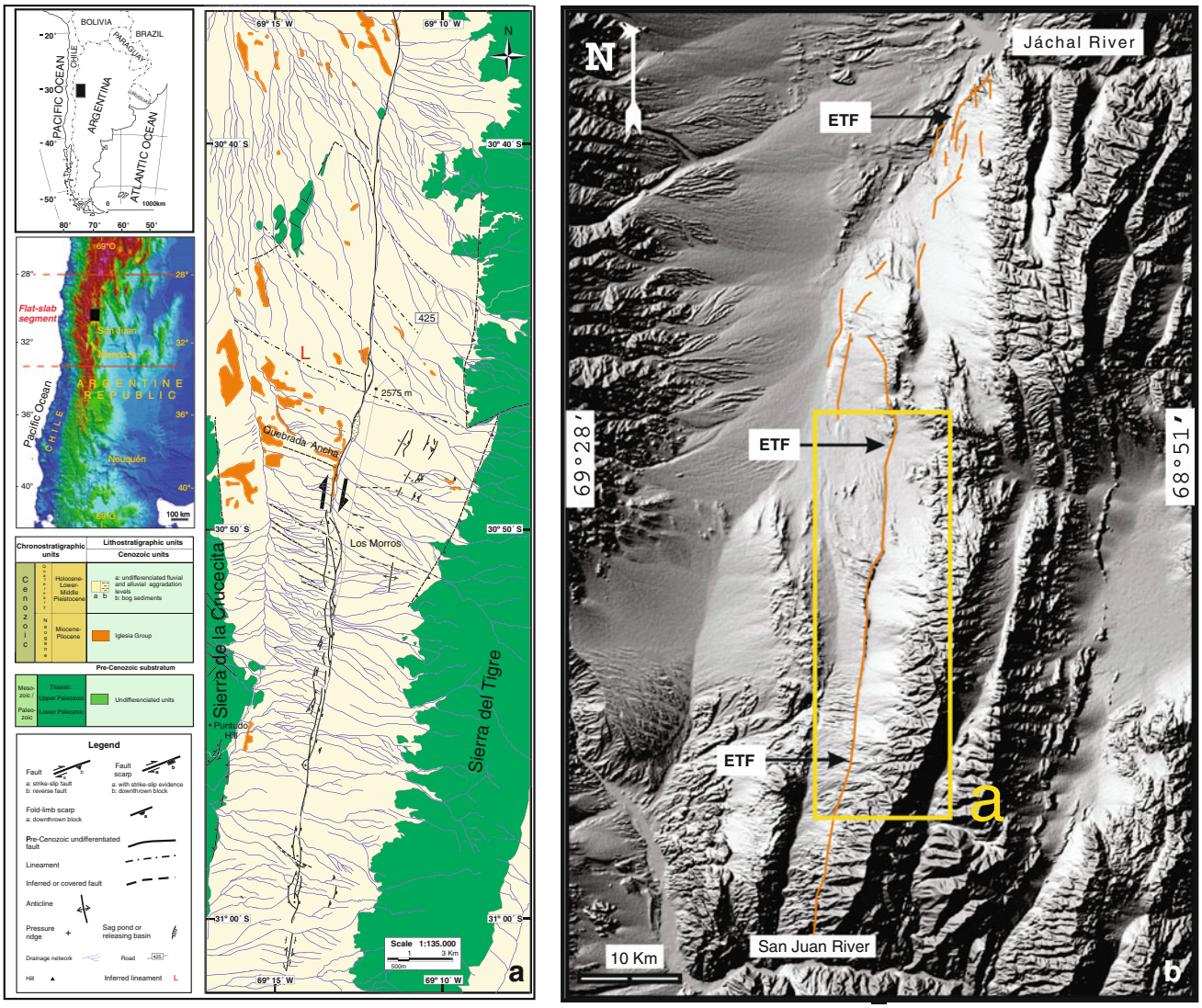

Fig. 1 **a** Geologic map and main structural features of the central part of the El Tigre Fault zone. **b** El Tigre Fault structure [following Siame et al. (1997b)] on digital elevation model (image from SRTM, 3 arc second, available at http://seamless.usgs.gov)

distributed outcrops of the Iglesia Group which represents a Neogene succession of continental sediments, volcanic and pyroclastic rocks. A few small Miocene andesitic intrusive bodies are also exposed in the area (Leveratto 1976). In the study region, the Neogene successions represented by the Iglesia Group are constituted by the Las Flores and Lomas del Campanario Formations (Wetten 1975a, b; Aparicio 1984; Weidmann et al. 1985; Contreras et al. 1990). According to published radiometric age data (Johnson et al. 1987; Re and Barredo 1993; Re 1994; Jordan et al. 1997), the age of the Iglesia Group is comprised between the Late Miocene (~11 Ma) and the Pliocene (~4 Ma). It is generally accepted that the Las Flores Formation overlies the Lomas del Campanario Formation by a regional unconformity (Contreras et al. 1990), although Gagliardo et al. (2001) considered that the two units interdigitate. The Lomas del Campanario Formation crops out in Cuesta del Viento, Lomas del Campanario and Iglesia, and is composed by ignimbrites, andesites, tuffs, agglomerates, conglomerates and sandstones. Good outcrops of the Las Flores Formation, composed of epiclastic and pyroclastic rocks, are present in the upthrown block of the El Tigre Fault (central sector, between 30°45′11″ and 30°49′08″) as part of the bedrock scarp and in the steep slope of the river valleys that entrench that scarp. Quaternary alluvial deposits infill the intermountain depressions, in the western piedmont of Sierra Negra and between Sierra de la Crucecita and Sierra del Tigre. Alluvial fans were studied in detail by Siame et al. (1997a, b), Siame (1998) and Yamín (2007). Taking into account the stratigraphical relations between the alluvial deposits, the presence of morphological surfaces and the results of minimum ^{10}Be exposure

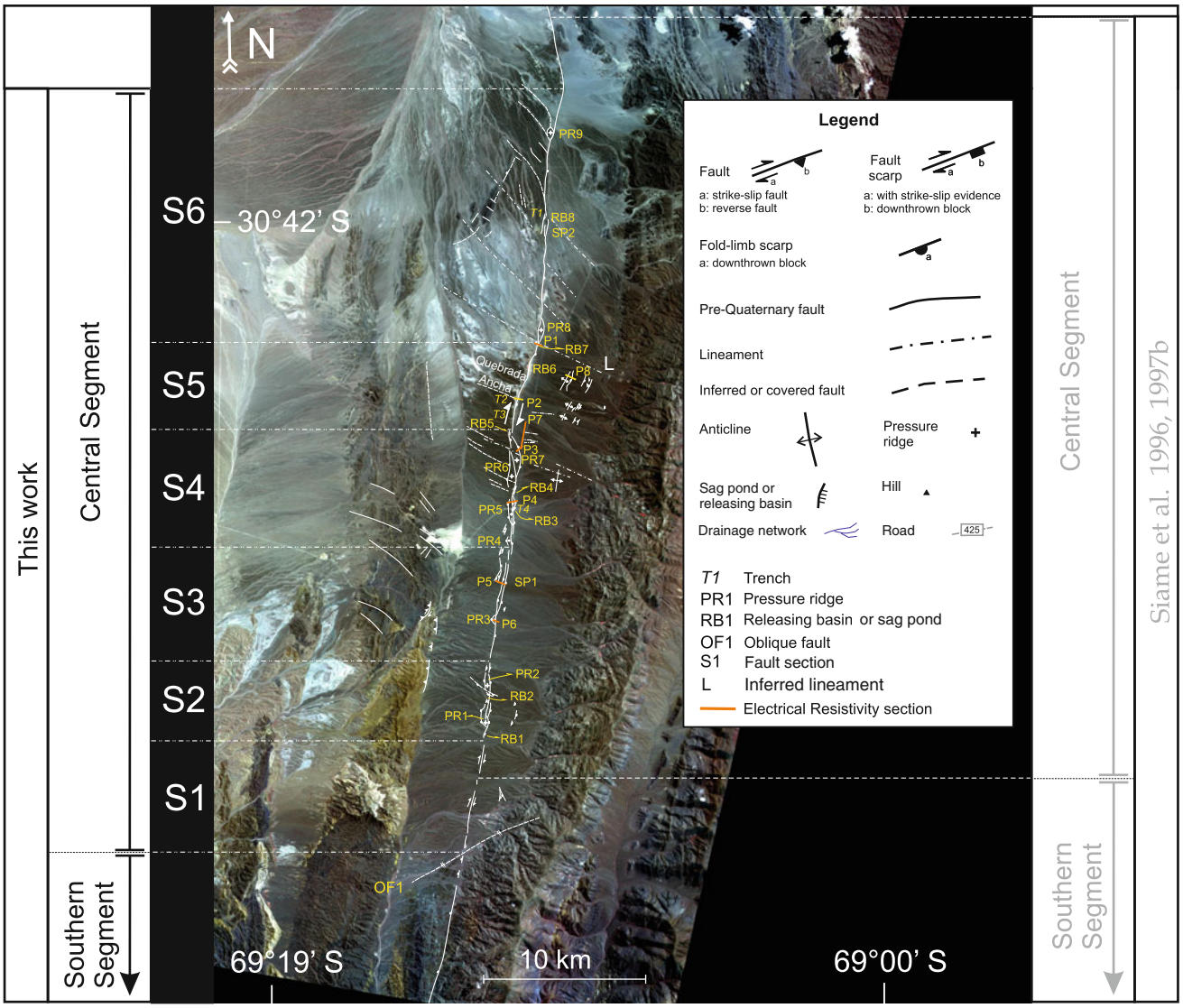

Fig. 2 Structure of the El Tigre Fault along the Central and Southern Segments on *top* of an ASTER satellite image (RGB: 321). The pressure ridges are marked as *PR*, releasing basins as *RB*, splays as *SP* and location of trenches as *T* (T1, T3 and T4 are approximate). Both segmentation proposals by Siame (1998) and this work are outlined. Locations of the eight geoelectrical profiles P1 to P8 are included

ages of alluvial-fan surfaces, the deposits were subdivided into six units (Siame et al. 1997a, b, Siame 1998), from (21 ± 4) ka to (670 ± 140) ka. Yamín (2007), on the other hand, only distinguished four regional levels of alluvial deposits and a fifth level represented by the recent sediments.

The El Tigre Fault

The El Tigre Fault has been characterized as a 120-km-long strike-slip fault with a major right-lateral strike-slip component and an uplifted western block on its central sector (INPRES 1982; Bastías and Bastías 1987; Bastías et al. 1990, 1993; Siame et al. 1996, 1997b, 2006; Cortés et al. 1999). Disruptions of Pleistocene surfaces and geomorphological features like fault scarps, releasing basins, pressure ridges and offset streams constitute the evidence for its Quaternary activity (Figs. 2, 3, 4). Pleistocene strata and Neogene successions of the Iglesia Group are affected by the fault, except for its southern ending where it affects the exposed Palaeozoic bedrock at Sierra del Tigre. The reverse east-vergent La Crucecita Fault that controls the uplift of the eponymous range, and the reverse faults that limit the eastern margin of Sierra del Tigre are the regional structures spatially associated with the El Tigre Fault (Cardó and Diaz 2005). Also, the western margin of Sierra del Tigre is controlled by a longitudinal structure, probably antithetic with the eastern thrusts that limit this range to the east, as suggested by satellite imagery and aerial photographs.

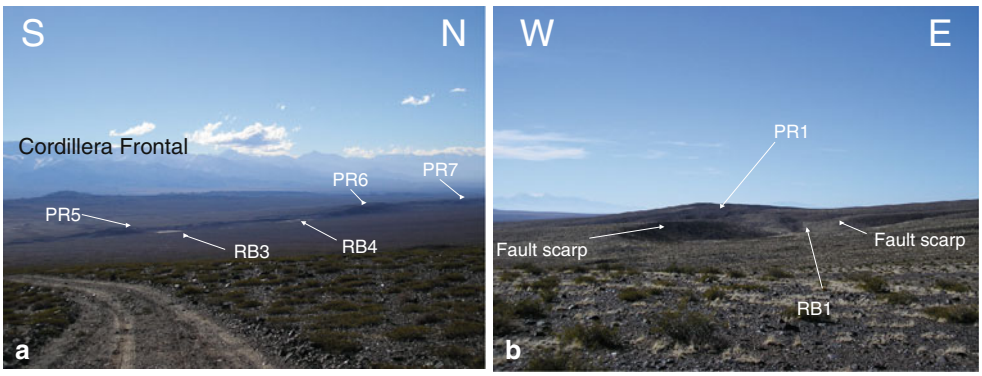

Fig. 3 **a** Panoramic sight from the east where several pressure ridges and releasing basins are observed (Central Segment). **b** Releasing basin (*RB1*) and pressure ridge (*PR1*) in the Southern Segment of the El Tigre Fault; view to the north. Scarps at the sides are recognized

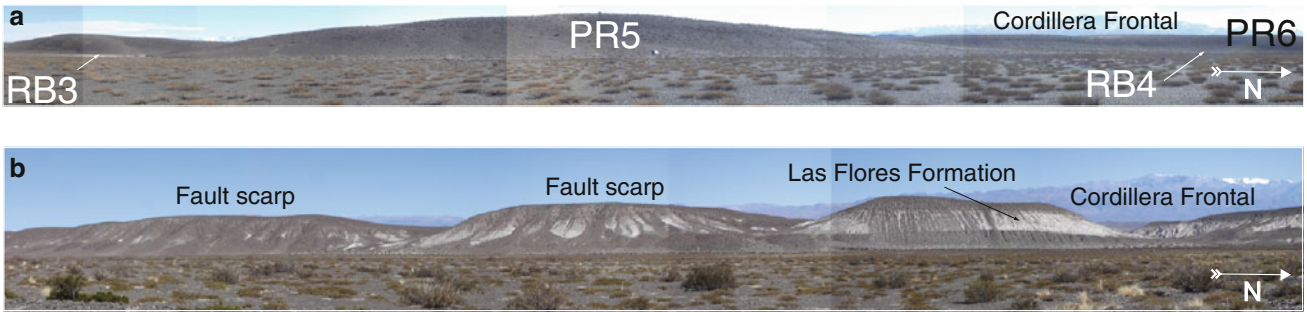

Fig. 4 **a** Piedmont and fold-limb scarps in the Central Segment of the El Tigre Fault. **b** Bedrock scarps (Central Segment); Las Flores Formation underlies the Quaternary alluvial deposits. Pressure ridges and releasing basins are identified

The actual extent of the El Tigre Fault has been the subject of important controversies. First studies proposed that it belongs to an extensive fault system of almost 1,000 km in length (INPRES 1982) called Caída del Tigre Fault. Later, Bastías et al. (1984), following this model estimated its length in roughly 800 km, extending the El Tigre Fault from Sierra de Cortaderas, in the Mendoza Province, to Laguna Brava, in the La Rioja Province (Bastías 1985). This long structure was also called the El Tigre Fault System composed of several individual faults as Agua del Jagüel, Jarillal, Tontal, El Tigre, Punilla, La Bolsa and Bonete (Bastías et al. 1985), Chaschuil, Aguas Calientes (Bastías and Bastías 1987), Cántaro de Oro, Infiernillos, Hilario, Carmen Alto, Puesto Tapia and La Cantera (Bastías et al. 1990). This model was adopted in many subsequent works: Bastías et al. (1985), Bastías (1985), Bastías and Bastías (1987), Bastías and Uliarte (1987), Paredes (1990), Bastías et al. (1990), Bastías (1990a, b), Abad et al. (1990), Paredes (1990), Cardó and Díaz (2005), Esper Angillieri (2007), among others. Nevertheless, other authors (Siame et al. 1996, 1997b, 2006; Cortés et al. 1999) have not found evidence of the El Tigre Fault extending beyond 120 km, neither to the north of the Jáchal River nor to the south of the San Juan River. In this interpretation, the other stated faults would not have any kinematic link with the El Tigre Fault. In this work, we assume that the latter fault model is valid.

Siame et al. (1996, 1997a, b, 2006) and Siame (1998) provided important contributions to the knowledge of the activity of the El Tigre Fault which included ^{10}Be cosmogenic dating of aggradation and erosion levels corresponding to Quaternary deposits affected by the fault activity. They recognized geomorphological markers which were used as evidence for right-lateral displacements, with a maximum offset of (260 ± 20) m cumulated during the Late Quaternary. The observed displaced surfaces have ages below ~700 ka (Siame et al. 1997b), which differs from the estimation presented by Bastías et al. (1985) and Bastías and Uliarte (1991), who stated that motions and strains are exclusively Holocene. The geological data indicate that the El Tigre Fault was mainly originated during the Middle Pleistocene, before the accumulation of the Late Pleistocene sediments. Then, during the Late Pleistocene and Holocene, the fault was reactivated generating smaller relief and displacements. Though pre-Quaternary activity cannot be completely ruled out in the central area of the fault, the geological evidence indicates null or scarce activity in this time due to the absence of an angular unconformity between the Neogene and Quaternary sediments. The age data and measurements

of cumulative horizontal and vertical displacements were used to calculate slip rates (Siame et al. 1997a, b), resulting in 1 and 0.3 mm/a, respectively. Siame et al. (1997b, 2006) have suggested that the El Tigre Fault is a major crustal-scale fault accommodating a dextral strike-slip component due to partitioning of deformation induced by the oblique convergence of the Nazca plate under South America. The presence of the east-facing steep slope in the Central Segment was interpreted by Siame et al. (1997b, 2006) as a result of oblique slip (rake 17°). According to these authors, the El Tigre Fault is strongly connected to the Precordilleran fold-and-thrust belt, in which slight strike variations seem to parallel the El Tigre Fault geometry and discontinuities (Siame et al. 1997b). If this interpretation is correct, both systems could be genetically related by partitioning the oblique convergence (3–8 mm/a shortening in the fold-and-thrust belt and 1-mm-dextral strike-slip displacement along the El Tigre Fault).

Considering the fault trace geometry, Siame et al. (1997b) proposed to divide the structure into three major segments: Northern (46 km long), Central (48 km long) and Southern (26 km long). The northern limit of the Southern Segment (31°01′30″S and 31°12′00″S, approximately) is located around 1 km to the south of two releasing basins (RB1 and RB2, Fig. 2), which are related to a double pressure ridge (PR1, PR2), whilst its southern extreme can be placed where the trace loses its geomorphological expression in the Palaeozoic rocks of Sierra del Tigre. This segment is characterized by a linear uninterrupted trace and a strike-slip component clearly evidenced by the right-lateral offset of the drainage network entrenching the alluvial fans that come from the western piedmont of Sierra del Tigre. This geomorphological marker has been used by Siame et al. (1997a, b) to measure the maximum accumulated displacement during the Quaternary and to calculate the horizontal displacement rate through combining the dating of different alluvial-fan surfaces.

The Central Segment has its northern limit where the fault bends to the northwest (~31°35′15″S) and has been recognized as a complex relay zone (Siame et al. 1997b). It can be distinguished by a clear piedmont and bedrock scarp with an east-facing slope which is the result of the vertical displacement along the fault (Fig. 4). This scarp has a slope of 18°–24° (Bastías et al. 1984) and, according to measurements by Siame et al. (1997b) and Siame (1998), a maximum height of approximately 85 m at Los Morros zone (Fig. 1a). Several transpressive and transtensive geomorphological features (pressure ridges and sag ponds, respectively) have been preserved on the western block of the fault (Figs. 2, 3, 4). Detailed geomorphological and geophysical studies were concentrated in this segment, which represent the main focus of this paper.

The Northern Segment has its northern edge in the Cuesta del Viento dam (~31°12′00″S) and was interpreted as a horse-tail–like termination of the El Tigre Fault due to the disperse rupture in several strands separated from 1 to 5 km (Siame et al. 1997b). Pérez and Costa (2006) described two major branches between the Negro Hill and the Jáchal River.

Previous geophysical prospection studies in the area affected by the El Tigre Fault are scarce. Some 2D reflection seismic lines have been reported from commercial oil industry exploration activities (Beer et al. 1990; Fernandez 1995; Re et al. 2003), but most of them are of poor quality or are unsuitable for the purpose of this study. Preliminary results of a geoelectrical survey were reported by Fazzito et al. (2009); near vertical to high-angle fault surfaces have been reported by interpreting four resistivity models which also suggest that this fault may act in some areas as a hydro-geological barrier.

The Central Segment of the El Tigre Fault

In the Central Segment (from 30° 47′07″S to 30° 49′08″S), the trace of the El Tigre Fault is recognized in the field as a main fault scarp usually of piedmont or, in part, bedrock nature, associated with pressure ridges, sag ponds and secondary branches (INPRES 1982; Bastías 1985; Bastías and Uliarte 1991; see Figs. 3a and 4). The drainage network coming from Sierra del Tigre on the east is related to the generation and development of alluvial fans and it is affected by the deformation associated with the El Tigre Fault. The vertical entrenchment of the drainage network in the younger alluvial fans is not significant, whilst in the older ones it becomes more evident (i.e. deeper). Most of these streams join major collectors parallel to the foot of the main scarp, until they follow through main west-striking antecedent valleys which outline water gaps. Other fluvial valleys, for which the entrenchment rate has been slower than tectonic uplifting, have become suspended in the upthrown block of the fault and appear as beheaded streams and several wind gaps. Also, the drainage appears shuttered in diverse releasing basins situated close to the scarp, as observed by Bastías et al. (1985), Bastías (1989), Bastías and Uliarte (1991) and Siame et al. (1997b). Along the whole Central Segment, there is a prominent dip-slip component of faulting, evidenced not only by the throw, but also by the beheaded rivers and the wind gaps that are preserved tens of metres over the foot of the scarp. As a result of the preservation of younger alluvial deposits close to the scarp in the eastern-downthrown block, the estimation of the horizontal slip rate of the fault from the offset of the landforms is not possible. This rate was estimated, though, in the Southern Segment from the offset stream channels (Siame et al. 1997a, b) as already mentioned.

Taking into account the evidence of landforms and palaeoseismological data, Bastías and Uliarte (1991) recognized that, between 30°30′S and 31°00′S, the El Tigre Fault has a combined oblique movement: a dextral strike slip with normal and reverse components evidenced by the geomorphological features. Some of the numerous landforms associated with right-lateral movement along the Central Segment of the El Tigre Fault were described by Bastías et al. (1985), Bastías (1989) and Bastías and Uliarte (1991). According to these authors, restraining bends are related to the presence of eight pressure ridges (not mapped), the internal structure of which would be that of a flower-like pattern of reverse faults. Releasing bends are associated with tectonic depressions or sag ponds inside the alluvial fans (releasing areas).

Four palaeoseismological trenches orthogonal to the fault trace were previously excavated in the Central Segment. Three of them (T1, T3 and T4, Fig. 2) have been carried out in bogs or sag ponds and presented 65° to 70° east-dipping fault planes (INPRES 1982; Whitney 1990). Siame (1998) identified four rupture surfaces at T2 (Fig. 2, 30°48′27″S, 69°13′09″W), of which the most important was a 78° east-dipping fault with a strike direction N17°E. In all cases, the identified faults record normal displacement associated with a local transtensive regime.

Structural and geomorphological observations

The analysis of aerial photographs (stereoscopic pairs at scale 1:50,000), ASTER satellite imagery (resolution: 15 m/pixel) and field observations permitted to identify and map fault trace discontinuities and diverse landforms of tectonic origin along the Central and Southern Segments of El Tigre Fault (see Figs. 1, 2).

Fault discontinuities

Transcurrent faults commonly show several geometrical discontinuities (Crone and Heller 1991) such as bends, stepovers and gaps (Woodcock and Fischer 1986; Woodcock and Schubert 1994), which are expressed as pressure ridges, sag ponds and pull-apart basins. The right-lateral strike-slip component of the El Tigre Fault, evidenced by the offset stream channels of the Southern Segment, determines that the pressure ridges are associated with left bends (restraining bends) whilst releasing basins and sag ponds are connected to right bends (releasing bends). There are also structural discontinuities (Crone and Heller 1991) like splays of hundreds of metres to a few kilometres long and intersections of the main fault with oblique structures (lineaments, inferred or covered faults). The splays are expressed in the field as steps or stepped scarps (multiple scarps, Stewart and Hancock 1991). Pressure ridges, releasing basins and splays are identified as PR, RB and SP in Fig. 2. Table 1 contains morphometric data of the pressure ridges (PR1–PR9, labelled from South to North) that were included in Fig. 2. Their width ranges from 300 to 550 m and their length varies between 0.58 and 2.3 km. The length/width ratio (from 1.57 to 6.0) indicates a prevalence of elongated forms (*spindle shaped*, Mann et al. 1983), instead of the more usual rhombohedral one. Nine releasing basins observed in the Central and Southern Segments (referred to as RB1 to RB9 in Fig. 2) display widths from 150 to 250 m and lengths from 250 to 750 m, with average values of 200 and 500 m, respectively. The average of the length/width ratio is 2.5, which also indicates a dominance of elongated landforms.

Sections along the El Tigre Fault

Boundaries of sections along the Central and Southern Segments of the El Tigre Fault have been defined where the major change in strike occurs. It has been observed that tectonic-related geomorphological features, such as sets of pressure ridges locally associated with small sag ponds, piedmont or bedrock scarps and splays, are not distributed homogeneously along the trace, but they variably characterize each section in relation to its strike.

In the Central and Southern Segments, six major sections (S1–S6, Fig. 2) were defined. The length of these sections ranges from 5.0 to 7.3 km, the strike of the fault along these sections varies from N–S to N18°E, whilst the strike variation between neighbouring sections ranges from 5° to 18°. Principal characteristics of each section are presented in Table 2. The disposition of landforms and the variations in strike enable us to interpret some of these strands as right or left large wavelength bends (several kilometres long) which define, respectively, major transtensive or transpressive sectors as a result of the right-lateral strike-slip motion along the fault. Sections S2 and S4 constitute major left bends, whereas S5 is a notable major right bend. These three sections represent major deflections of the fault trace. The main transpressive areas comprise associations of pressure ridges and small sag ponds distributed among them. The ridges can be aligned (S2) or overlapping and imbricated (S4) in restraining duplexes caused by strike-slip faulting (Woodcock and Fischer 1986). The other sections, with no or few isolated pressure ridges or releasing basins, show generally bedrock or piedmont scarps and splays (S1, S3, S6) and do not constitute prominent inflexions. The S1 section shows a prominent strike-slip behaviour with a linear trace (Bastías 1985; Siame et al. 1997b) and a null or small dip-slip component (a restraining component due to the presence of an in line pressure ridge in the trace could be inferred). Section S6 presents one releasing basin and two pressure

Table 1 Morphometrical details of the features (pressure ridges) along the Southern Segment and the Central Segment of the El Tigre Fault

Pressure ridge	Coordinates		Length (km)	Width (km)	Length/width ratio
	South latitude	West longitude			
PR1	30°59′11″	69°14′31″	1.50	0.45	3.33
PR2	30°58′25″	69°14′19″	1.50	0.40	3.75
PR3	30°56′06″	69°14′06″	0.50	0.30	1.67
PR4	30°53′12″	69°13′24″	1.00	0.30	3.33
PR5	30°52′01″	69°13′26″	1.80	0.30	6.00
PR6	30°51′06″	69°13′24″	2.20	0.50	4.40
PR7	30°50′27″	69°13′12″	2.20	0.55	4.00
PR8	30°46′05″	69°12′14″	1.70	0.40	4.25
PR9	30°39′17″	69°11′50″	0.58	0.37	1.57
Range of variation			0.50–2.20	0.30–0.55	1.57–6.00
Average values			1.44	0.40	3.59

They are enumerated from PR1 to PR9, from south to north

Table 2 Sections in the Central and Southern Segments, named from S1 to S6 from south to north

Segment (Siame et al. 1997b)	Section	Landforms and structures	Length (km)	Average strike of the section	Angle between sections	Dominant inferred stress regime
Southern		Segment south of the fault OF1				
Southern	S1	Strike-slip fault scarps	7.5	N10°E	S1–S2: 5°	Transcurrent
		Offset stream channels				
Central	S2	PR1, PR2, RB1, RB2	5.0	N5°E	S2–S3: 5°	Transpressive
Central	S3	Piedmont scarps	7.5	N10°E	S3–S4: 10°	Transtensive?
		Splays				
		SP1				
		PR3				
Central	S4	Piedmont and fold-limb scarps	7.5	N–S	S4–S5: 18°	Transpressive
		PR4, PR5, PR6, PR7, RB3, RB4, RB5				
Central	S5	Piedmont and bedrock scarps	5.5	N18°E	S5–S6: 13°	Transtensive
		RB6, RB7				
Central	S6	Bedrock and piedmont scarps	16.0	N5°E		Transpressive
		Splays				
		PR8, PR9, SP2, RB8				

Geometric data and type of dominant stress regime by sectors are indicated

ridges, all of them isolated and related to local small inflections of the fault. In its northern tip, the R2 splay (upthrown block) presents left bending with a progressive uplift of pre-Cenozoic bedrock blocks, suggesting a transpressive tectonic regime. Confirmation of the inferred transtensive or transpressive character of the stress regime in some of these sections (S3, S4, S5; Table 2) was one of the main objectives of the geophysical surveys carried out.

Minor geometrical discontinuities have been also identified and are represented by left bends, which have associated pressure ridges from 1 to 2.3 km long, or right bends and stepovers, which related releasing basins varying from 250 to 750 m in length. The releasing basins are in general associated with sag ponds limited by a main fault scarp in their western margin. In the present work, the subsurface structure of two pressure ridges and one releasing basin, along the S3, S4 and S5 sections, were studied through the electrical resistivity tomography (ERT) method.

Transverse and oblique structures

The longitudinal continuity of the Quaternary deposits in the piedmont of Sierra del Tigre is disrupted by an oblique fault with a N70°E direction (indicated as OF1 in Fig. 2) which uplifts blocks of the Palaeozoic bedrock to the south within the intermountain valley. In the same way, the

Central and Southern Segments of El Tigre Fault are crossed by several transverse and oblique faults, mostly with WNW–ESE (N110°/114°E) and NW–SE (N134°/136°E) strike (see Fig. 2). They comprise inferred faults and lineaments revealed by long linear strands of stream channels that do not expose the bedrock on surface, as opposed to the OF1 fault. These features seem to play an important role in the kinematics of different sections of the El Tigre Fault. They are not distributed uniformly but concentrated in specific areas, for example, within the sections S4, S5 and S6. Several NW–SE trending lineaments and faults were inferred to the north of the Quebrada Ancha (Figs. 1, 2) from the linear pattern of the drainage network drawing a horse-tail pattern at the northern end of the Central Segment. In the area between Los Morros and Quebrada Ancha, on the downthrown block, WNW–ESE trending gentle piedmont scarps cut the alluvial-fan deposits and control the drainage network. These structures were studied by an ERT profile (P7 cross-cut, Fig. 2). A lot of pre-Quaternary NW–SE trending fractures exposed in the Palaeozoic basement were mapped at Sierra de la Crucecita next to the S3 and S4 sections, suggesting that NW–SE trending Quaternary faults and lineaments are likely controlled by, and represent reactivations of, inherited structures.

An inferred lineament (L), between the RB7 releasing basin and the PR8 pressure ridge (Figs. 1, 2), represents another oblique structure, which is apparently of significant kinematic importance. The main geological characteristics observed around this structural feature are: to the south of L, (a) a greater throw of the El Tigre Fault, (b) the lack of the oldest Quaternary alluvial deposits (age between (670 ± 140) ka and (180 ± 38) ka, Siame et al. 1997a, b) over the eastern block, (c) the presence of a large sedimentary basin (RB6), (d) a remarkable change in the drainage network from an NW orientation to the north of L to a WNW orientation to the south of L, and to the north of L, (e) exposures of folded rocks of the Las Flores Formation that are only slightly tilted to the south. This lineament may thus represent a major structural boundary separating two areas with different kinematics and might represent an inherited basement structure controlling locally the behaviour of the El Tigre Fault.

Minor structures to the east of the El Tigre Fault

Tectonic features of minor dimension were localized over the eastern block of the El Tigre Fault, in the piedmont plain of Sierra del Tigre. These structures affect exclusively ancient Quaternary alluvial deposits (see Figs. 1, 2). They are localized from 1 to 2 km to the east of the El Tigre Fault trace and do not have any surficial direct contact with it or mechanical soft linkage. They are east- or west-facing piedmont fault scarps and gentle anticlines subparallel or slightly oblique to the El Tigre Fault trace of hectometric dimensions. A greater concentration of these structures is observed at the latitude of Quebrada Ancha (Figs. 1, 2). We will further discuss these features in a subsequent section where, based on the results of the geophysical survey, it is suggested that these structures are likely parts of splays connected to the Sierra del Tigre backthrust and not to the El Tigre Fault.

The segmentation of the El Tigre Fault

Taking into consideration the structural observations presented in this work, we reconsider the geometrical segmentation model of the El Tigre Fault adopted by Siame et al. (1997b), suggesting minor changes. The new boundaries between segments here determined take into account the geometry, structure and behaviour of each segment in order to represent a better estimation of the possible co-seismic rupture behaviour. The boundary between the Northern and the Central Segments is considered to be 5.5 km to the south from that proposed by Siame et al. (1997b), at 30°38′00′S, where the fault bifurcates into two branches, one with an NW strike (Fig. 2). Furthermore, the boundary between the Central and the Southern Segments is assumed in correspondence with the intersection with the OF1 oblique fault, whilst the limit considered by Siame et al. (1997b) was defined in the vicinity of PR1 and PR2 pressure ridges. This intersection represents an irregularity of first order that strongly affects the morphotectonic configuration of the El Tigre Fault. The OF1 fault controls the uplift of the pre-Cenozoic bedrock in the intermountain valley between Sierra de la Crucecita and Sierra del Tigre. To the south of this structure, the alluvial deposits are significantly reduced in their extension and the El Tigre Fault appears as the western boundary of the Sierra del Tigre range. The Southern Segment would, therefore, be confined only to the highland portion. Under these conditions, the length of the Northern Segment is 52 km, that of the Central Segment 49 km and that of the Southern Segment 20 km if we assume that the fault ends at the San Juan River, though we cannot definitely rule out a possible extension farther south. Despite this redefinition of the boundaries, the new segmentation does not introduce any significant difference in the magnitudes of the maximum expected earthquake per segment as calculated by Siame et al. (1997b) according to the Hanks and Kanamori scaling laws (1979): 7.1 ± 0.1 for the Central Segment and 6.9 ± 0.1 for the Southern Segment.

2D ERTs

The application of the 2D ERT method for modelling geological bodies and characterizing Quaternary faults has led to encouraging results as already published in the last decade (e.g. Fleta et al. 2000; Giano et al. 2000; Storz et al. 2000; Suzuki et al. 2000; Verbeeck et al. 2000; Demanet et al. 2001a, b; Caputo et al. 2003, 2007; Wise et al. 2003; Colella et al. 2004; Rizzo et al. 2004; Nguyen et al. 2005, 2007; Fazzito et al. 2006, 2009; Terrizzano et al. 2008, 2010, 2012; Nivière et al. 2008; Pánek et al. 2011). In the present study, the main objective of applying this methodology has been to provide information on the subsurface geometry of the El Tigre Fault in its Central Segment. The survey was carried out with a Syscal R1 Plus Switch 48 Plus Georesistivity-meter (Iris Company) with 48 electrodes normally spaced at 10 m. The resistivity meter is able to automatically perform a predefined set of measurements according to a suitable type of arrangement and stores the data of average transmitted current, average reception voltage, location of electrodes, apparent resistivity values and related standard deviation for each defined quadripole.

Of the eight ERTs that were carried out, six are orthogonal to the El Tigre Fault, which they cross about their middle points. These are distributed along the three major sections of the Central Segment: S5 (P1 and P2 surveys), S4 (P3 and P4 surveys) and S3 (P5 and P6 surveys). Another profile runs parallel to the main fault (P7 survey) surveying the northern part of S4 and the southern of S5. The last profile was carried out across some minor structures over the piedmont of Sierra del Tigre (P8 survey). All ERTs included in this work, with the exception of P7, have been performed with a dipole–dipole array. It is accepted that this option provides good horizontal resolution in resistivity surveys (Loke 1996–2011) and therefore it is more appropriate for imaging subvertical faults (Caputo et al. 2007; Nivière et al. 2008; Fazzito et al. 2009; Pánek et al. 2011; Terrizzano et al. 2012). For P7, a Wenner–Schlumberger array was chosen to exploit the greater vertical sensibility in order to emphasize the layering of the alluvial deposits. The electrode nodes were equally spaced every 10 m for the basic arrangement (i.e. the total length of the electrical array was 470 m). In some occasions (P4, P5, P7, P8), the basic array was further extended by means of the *roll-along* technique. The location of the eight geoelectrical profiles (P1–P8) is presented in Fig. 2 and specified in Table 3; measurement parameters are listed in Table 4.

The pseudoresistivity measurements are conventionally arranged in the form of pseudosections or pseudodepth plot (Telford et al. 1990). These are contour colour fill diagrams of pseudoresistivity values where the horizontal axis represents the geometrical midpoint of a quadripole and the vertical axis corresponds to the pseudodepth value. Apparent resistivity values with standard deviation over 4 % were discarded. This criterion implied that the percentage of actual data that was kept for resistivity modelling was 93 % in average.

Table 3 Strike and coordinates of the midpoint for P1 to P8 survey lines

Survey	Coordinates of the midpoint of the survey lines		Strike
	South latitude	West longitude	
P1	30°46′29.4″	69°12′20.5″	N113°E
P2	30°48′28.0″	69°13′08.4″	N110°E
P3	30°50′13.4″	69°13′05.5″	N62°E
P4	30°51′58.8″	69°13′21.0″	N84°E
P5	30°54′45.5″	69°13′49.6″	N112°E
P6	30°56′05.3″	69°14′03.6″	N105°E
P7	30°49′44.4″	69°12′56.1″	N10°E
P8	30°47′40.2″	69°11′05.7″	N116°E

For this research, the resistivity modelling was solved numerically through the RES2DINV software (Geotomo; Loke 2001; Loke 1996–2011). This model consists essentially of rectangular cells of constant resistivity that adjust the pseudoresistivity values measured at the surface up to an acceptable error. Typically, the dimension of the cells is related to a multiple of the electrode spacing. Concerning the model discretization, for the presented models, the cell has been set to a width that is equal to the minimum electrode separation (10 m) and a cell height that increases by 10 % in each deeper layer (this option is chosen to admit the loss of resolution of the geophysical method with depth). Concerning the matter of the non-uniqueness in the geophysical problem, we have made the assumption that resistivity values change smoothly in order to reduce the number of possible solutions. For the forward model subroutine, the finite-element method has been used. The discrepancy (*misfit*) between the calculated values of apparent resistivity and those inferred from field data are expressed through the root mean square (RMS) which varied approximately from 4 to 14 %, after 3 to 5 iterations. For every electrical survey, it has been observed that the calculated pseudosection is roughly similar to the pseudosection corresponding to the field measurements and differ only in minor features. The topographic information, collected in general every ten metres with a barometric altimeter, was incorporated into the models by a uniformly distorted grid (all the grid nodes along the same vertical line are shifted the same distance according to the elevation of the ground surface). The results of the ERTs are described and shown in the following section. Four of them

Table 4 Geometrical and acquisition parameters used in each survey line

Survey	Array type	Potential dipole length (m)	Depth level *n*	Section length (m)	Number of quadripoles	Current pulse duration (s)	Stack min–max	Expected standard deviation (%)	Maximum investigation depth of the 2D model (m)
P1	DD	10	1–6	470	545	1	2–5	5	61
		20	3–12						
P2	DD	10	1–6	470	589	1	2–4	3	50
		20	3,7/2,4,9/2,5,11/2,6						
		30	4,13/3,14,3,5,16/3,17/3,6						
P3	DD	10	1–6	470	503	1	2–6	5	50
		20	3–10						
P4	DD (ra)	10	1–6	710	1,188	1	2–4	3	50
		20	3,7/2,4,9/2,5,11/2,6						
		30	4,13/3,14,3,5,16/3,17/3,6						
P5	DD (ra)	10	1–6	710	867	1	2–6	5	51
		20	3–10						
P6	DD	10	1–6	470	545	1	2–6	5	51
		20	3–12						
P7	WS (ra)	10	1–6	1,910	2,881	1	2–4	3	50
		20	3,7/2,4,9/2,5,11/2,6						
		30	4,13/3,14,3,5,16/3,17/3,6,19/3,20/3,7						
P8	DD (ra)	10	1–6	710	1,322	1	2–4	3	51
		20	3,7/2,4,9/2,5,11/2,6						
		30	4,13/3,14,3,5,16/3,17/3,6,19/3,20/3,7						

It is also specified the maximum penetration depth of the numerical 2D resistivity model. The dipole–dipole array is indicated as DD, the Wenner–Schlumberger array as WS and "ra" points out the use of the roll-along method

(corresponding to P1, P3, P5 and P6 surveys) have already been published in Fazzito et al. (2009).

Results

Section S5

The S5 section is characterized by a N18°E-trending 5.5 km-long bedrock or piedmont scarp and is associated with two releasing basins (RB6 and RB7, Fig. 2) developed on the downthrown block. Two ERTs were obtained in this section: P1 across RB7 (Fig. 5a) and P2 (Fig. 5b) also orthogonal to the fault scarp and parallel to the palaeoseismological trench excavated and analysed by Siame (1998), where evidence of small scale normal faulting associated with the main fault has been described at this trench.

The 470-m-long P1 survey lies along a stream channel approximately orthogonal to the fault trace. The tomographic model (Fig. 6a) has been described extensively in Fazzito et al. (2009). It reveals a resistivity discontinuity immediately below the inferred position of the scarp ($x = 140$ m) which has been obliterated by a principal stream but can be easily interpolated from the scarp at both sides of the creek. This discontinuity in the resistivity is interpreted to reflect a subvertical fault plane, which is also characterized by a relatively broad zone with very low resistivity ($\rho < 15$ Ωm). An associated blind fault is suggested some 30 m towards the east of the main fault by a significant drop in the resistivity values. Distribution of resistivity values on the eastern half of the model are interpreted to reflect the stratification of the alluvial sediments in the eastern block, which seem to dip gently towards the east, that is, against the natural slope of the Sierra del Tigre piedmont.

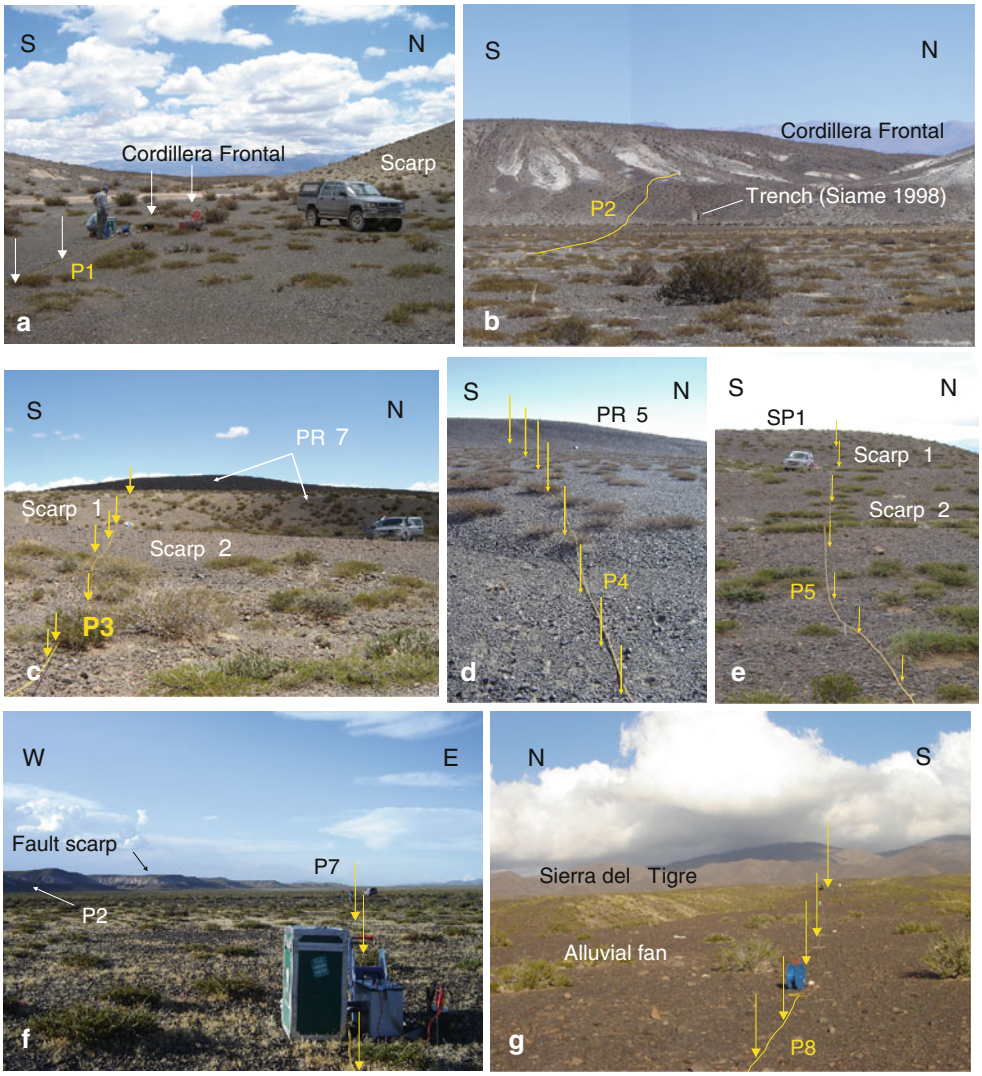

Fig. 5 Linear arrays for geoelectrical surveys (indicated by *arrows*) that cross-cuts the El Tigre Fault trace, oblique and minor structures

P2 runs 5 m to the north of the trench excavated by Siame (1998) and 3.8 km to the south of P1. According to this ERT (Fig. 6b), a highly resistive zone ($\rho > 500$ Ωm) approximately 20 m thick extends from the eastern end of the profile up to $x = 190$ m where it is abruptly interrupted. This interruption approximately coincides with the base of the fault scarp. The highly resistive level continues also in the upthrown block, having roughly a similar thickness, but at a higher topographic level as a consequence of displacement along the fault plane. Some thinning close to the scarp is observed which may suggest some erosion process or less deposition. To the east and under the high resistive zone, there is a conductive level ($\rho < 90$ Ωm) that is clearly interrupted below the front of the fault scarp ($x = 190$ m). The location of this discontinuity corresponds as well to that of the main rupture observed in the trench (Siame 1998). So, the ERT indicates the presence of an east-dipping fault ($x = 190$ m) confirming a normal slip component of the El Tigre Fault along this section, in agreement with the dip of a minor fault associated with the main fault zone observed in the palaeoseismological trench (Siame 1998). The conductive layer may correspond to the water table, which would corroborate the important hydro-geological control of the fault zone at the site. The presence of a major ditch along the fault trace between P1 and P2, which works as a water reservoir for the whole area, is also evidence of such control. Resistivity stratification in the downthrown block dips slightly to the east, as in P1, against the regional slope. This confirms a small but significant tectonic tilting of the down-thrown block associated with the activity of the El Tigre Fault all along section S5. As example, we have chosen this survey to show additional data concerning the measured pseudosection, the calculated pseudosection and

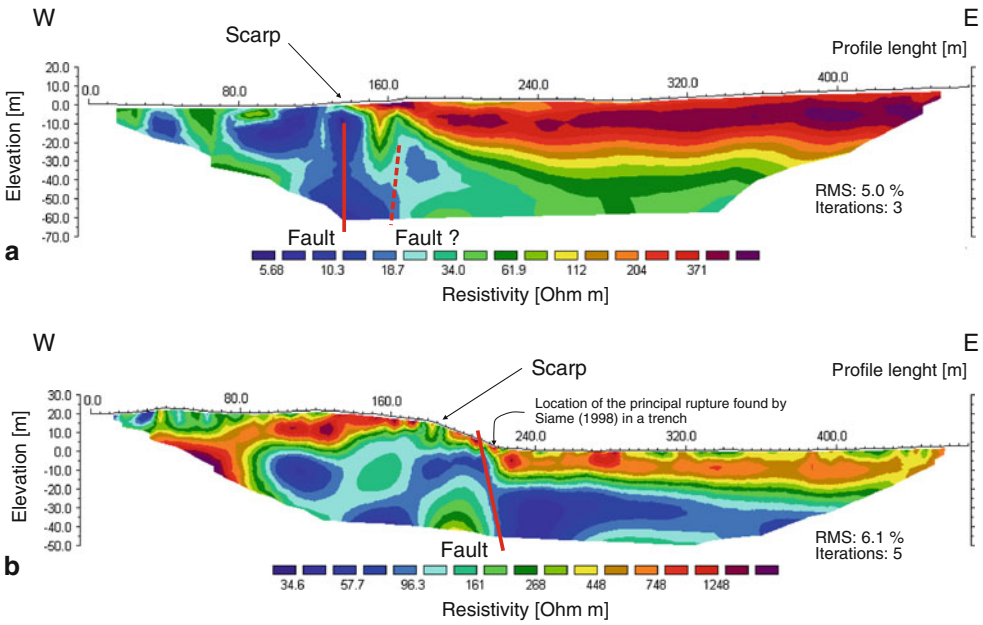

Fig. 6 **a** Electrical resistivity tomography that cross-cuts the main structure of the El Tigre Fault at P1 (*array*: dipole–dipole; minimum unit electrode spacing: 10 m; smooth inversion; maximum penetration depth: 61 m). More details for this profile were presented by Fazzito et al. (2009). **b** Resistivity model with topography corresponding to the P2 survey that cross-cuts the El Tigre Fault (*array*: dipole–dipole; roll-along method; minimum unit electrode spacing: 10 m; smooth inversion; maximum penetration depth: 50 m). More details in the text

the resistivity block models (see Fig. A of Electronic Supplementary Material 1).

Section S4

Section S4, characterized by piedmont and fold-limb scarps, has two associations of pressure ridges (PR4 with PR5 and PR6 with PR7) and three small sag ponds (RB3, RB4 and RB5).

The ERT P3 is located 3.3 km to the south of P2 and cross-cuts the pressure ridge PR7. This 470-m-long survey includes a fold-limb scarp (Scarp 1 in Fig. 5c) and a second scarp of fluvial origin (Scarp 2). The resistivity model corresponding to this profile (Fig. 7a, also described in detail in Fazzito et al. 2009), shows a west-dipping high-angle conductive zone at $x = 210$ m, just below the fold-limb scarp, suggesting that the pressure ridge structure is bounded to the east by a west-dipping fault. At the top of the downthrown block, the alluvial sediments ($\rho > 200$ Ωm) lay, again, against the regional slope, though layering is poorly defined. Two possible blind faults have been also inferred to the east of the main fault from resistivity discontinuities. In this case, the fault seems to have a lesser effect on the continuity of the water table.

The P4 survey (Fig. 5d), across the PR7 pressure ridge, was located approximately 3.3 km to the south of P3. The section is 710 m long and the maximum penetration depth of the survey, approximately 50 m. The resistivity model (Fig. 7b) shows a highly resistive ($\rho > 550$ Ωm) western block associated with the structure of the pressure ridge approximately up to $x = 400$ m. According to the model, the sedimentary units that constitute the pressure ridge are slightly folded forming a broad anticline. This part of the ERT differs clearly from the much less resistive eastern block ($\rho < 500$ Ωm, $x > 400$ m) probably due to an important lithological difference. In this profile, the fault zone is inferred mainly by the sharp contrast in the resistivity values and the presence of a broad more conductive zone ($\rho < 200$ Ωm). This subsurface contrast coincides at surface with the fault-limb scarp ($x = 400$ m). Although no narrow conductive zone can be assigned to reflect the fault plane, a high-angle west-dipping fault plane has been interpreted (reverse fault). The high-resistivity contrast between the western and eastern blocks and the presence of low resistivity values in the fault zone suggest again that the fault acts as a hydro-geological barrier to the aquifer fed by the Sierra del Tigre. The model also shows lack of evidence of any secondary fault bounding the pressure ridge on the west. This is against a model of the pressure ridge produced by a positive flower structure in a transpressive zone, as previously proposed in a general way by Bastías and Uliarte (1991).

Section S3

Section S3 of the El Tigre Fault is dominated by a piedmont scarp with a widespread splay (R1) and a small pressure ridge (PR3, Fig. 2). Two resistivity profiles were acquired in this section and were exhaustively described in a previous work (Fazzito et al. 2009), so here, only the most important remarks will be pointed out.

The ERT P5 is 710 m long and it is located 5.2 km south of P4. It runs across a multiple scarp (Fig. 5e), with two highs, the eastern one being the most recent, since it affects the youngest sediments and has a lower elevation. A major discontinuity in the resistivity pattern (Fig. 8a) is

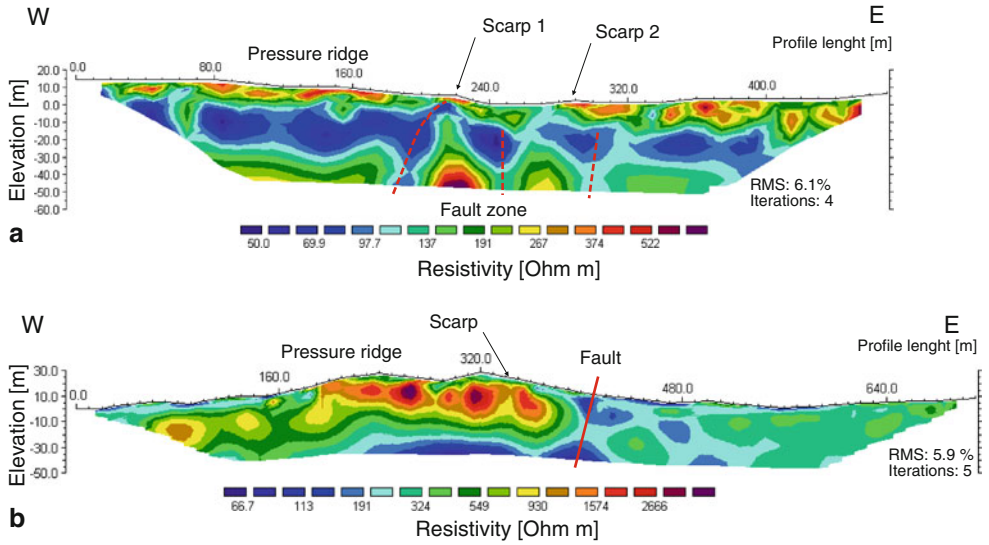

Fig. 7 **a** Electrical resistivity tomography associated with the P3 survey (*array*: dipole–dipole; minimum unit electrode spacing: 10 m; smooth inversion; maximum penetration depth: 50 m). More details for this profile were presented by Fazzito et al. (2009). **b** P4 resistivity model carried out across El Tigre Fault (*array*: dipole–dipole; minimum unit electrode spacing: 10 m; smooth inversion; maximum penetration depth: 50 m)

evident at $x = 500$ m in coincidence with Scarp 2. Its location and character suggest a subvertical fault. Two less important discontinuities are apparent at $x = 270$ m and $x = 390$ m. They do not correspond to any special surficial feature and therefore their meaning is difficult to be established. They have been speculatively interpreted as possible blind faults. Scarp 1 is located over 50 m westwards from the easternmost "blind fault", so that if they are related it would mean a very important erosional recession of the scarp and a long inactivity. Whether this is likely it is at least dubious.

The ERT P6 is located 2.6 km to the south of P5 and cross-cuts the PR3 pressure ridge. Here, the resistivity model (Fig. 8b), 470 m long and 50 m deep, shows a very clear discontinuity ($x = 220$ m) at the eastern boundary of the pressure ridge, just below the fold-limb scarp. The resistivity pattern is interpreted as due to a high-angle west-dipping fault (reverse fault). The eastern, downthrown, block shows relatively low resistivity values characteristic of the alluvial deposits ($\rho > 150$ Ωm) that constitute the piedmont of Sierra del Tigre and suggest layering against the regional slope. The low resistivity level in the eastern block ($x > 220$ m, $z < -40$ m, $\rho < 100$ Ωm) that reflects high water content is abruptly interrupted at the inferred fault plane, providing further evidence of the hydro-geological control exerted by the El Tigre Fault. No significant geoelectrical structure is evident on the upthrown (western) block. This is consistent with a pressure ridge not corresponding to a positive flower structure, as it was also seen in previously discussed ERTs.

Longitudinal survey: P7

The P7 ERT (Fig. 5f) has its southern tip in the proximity of the PR7 pressure ridge (30°49.3′S), where a local but significant change in strike of the main fault trace can be observed (from N5°W to N9°E), and it cuts across the P3 survey at $x = 325$ m. Its orientation is roughly parallel to the El Tigre Fault (N9°E). Its extension of 1,910 m was achieved via the roll-along method and it was the only tomographic survey done with a Wenner–Schlumberger configuration. The resistivity model reached a maximum penetration depth of 50 m and mainly shows a lateral homogeneity in resistivity values without abrupt transitions. Along the whole profile (Fig. 9), a high-resistivity shallow level ($\rho > 350$ Ωm) reaches a typical depth of 10 m. However, between $x = 880$ m and $x = 1{,}230$ m, this level deepens up to approximately 20 m and shows a slight increase in resistivity. Under this shallow level, the subsurface is characterized by lower resistivities, generally between 150 and 200 Ωm. However, under the central area ($880 \text{ m} < x < 1{,}230$ m), a much more conductive layer is evident, with resistivity values well below 100 Ωm, suggesting possibly a larger concentration of underground water. The important increase in the thickness of the alluvial coverage and the disposition of the resistivity contours suggest the occurrence of two antithetic normal faults bounding the central block thus defining a small graben-like structure without significant superficial expression. Figure 10 shows an

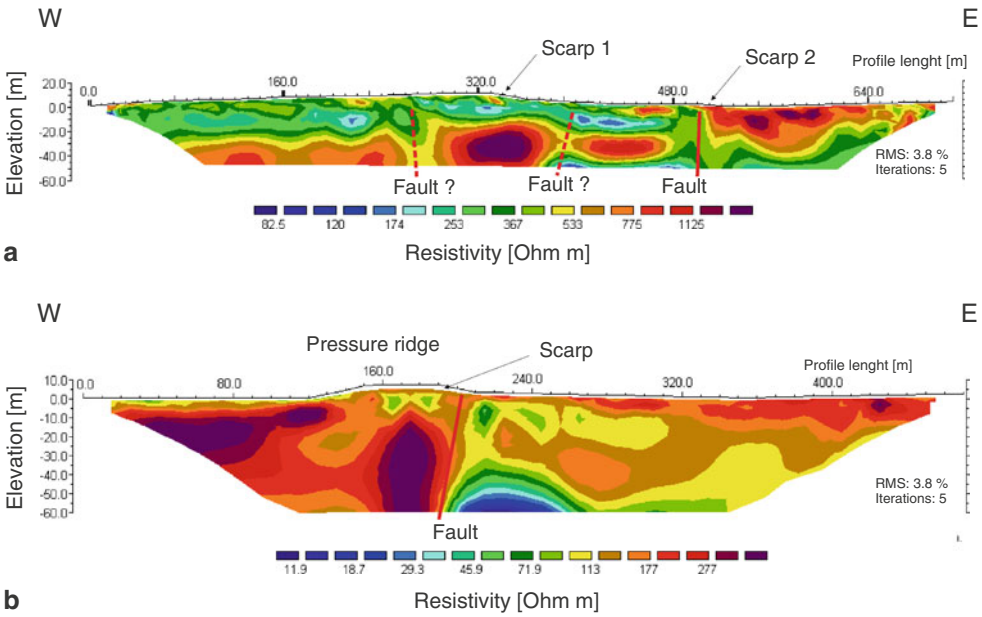

Fig. 8 **a** The P5 electrical resistivity tomography cross-cuts the main structure of the El Tigre Fault (*array*: dipole–dipole; minimum unit electrode spacing: 10 m; smooth inversion; maximum penetration depth: 51 m). More details for this profile were presented by Fazzito et al. (2009). **b** Resistivity model corresponding to the P6 survey that cross-cuts the El Tigre Fault (*array*: dipole–dipole; roll-along method; minimum unit electrode spacing: 10 m; smooth inversion; maximum penetration depth: 51 m). More details for this were presented by Fazzito et al. (2009)

ASTER image of the area surveyed by P7. Several lineaments approximately orthogonal to the El Tigre Fault can be observed. One of them intersects the P7 ERT at $x = 1{,}230$ m, therefore strongly suggesting it could correspond to the interpreted normal fault in the subsurface.

Minor structures: P8

The P8 survey (Fig. 5g) was carried out on the western piedmont of Sierra del Tigre at the latitude of Quebrada Ancha. It is located on top of a very gentle bulge of the piedmont surface limited by small scarps that affect the alluvial fans, interpreted as an incipient fold structure of tectonic origin. The survey, with a N115°E trend (i.e. almost orthogonal to the El Tigre Fault trace) is located at 2.5 km to the east of the fault. The 710-m-long ERT was recorded with the dipole–dipole method and its model reached a depth of about 60 m. In this resistivity model (Fig. 11), a shallow resistive level ($\rho > 250$ Ωm) characterizes the whole profile with a normal depth of 10 to 20 m which increases to approximately 40 m between $x = 260$ m and $x = 570$ m. The latter zone is bounded at the surface by two fault scarps both facing to the west (Scarp 1 and Scarp 2). The interpretation of the resistivity model is not straightforward, and speculatively two high-angle east-dipping faults are proposed as limiting the thickened resistive zone also in coincidence with the topographic scarps. However, it must be accepted that the usual features used in previous models to identify the presence of faults (abrupt resistivity contrasts, narrow subvertical conductive zones, etc.) are more ambiguous here. If the tectonic interpretation is correct, it would suggest that neotectonic activity in this area of Sierra del Tigre piedmont is more likely related to western back-thrusts of this range than to the motion of the El Tigre Fault. The presence of the water table at depths of 40 to 50 m below surface is inferred from very low resistivity values ($\rho < 40$ Ωm) at the bottom of the whole cross section. Further, systematic geomorphologic and geophysical studies are needed to characterize better the Quaternary tectonic activity at this piedmont.

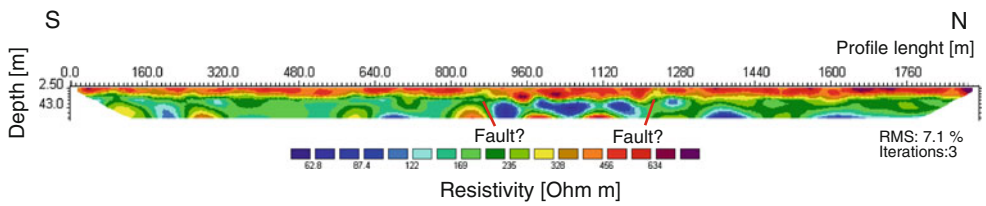

Fig. 9 P7 electrical resistivity tomography parallel to the El Tigre Fault (*array*: Wenner–Schlumberger; roll-along method; minimum unit electrode spacing: 10 m; smooth inversion; maximum penetration depth: 50 m)

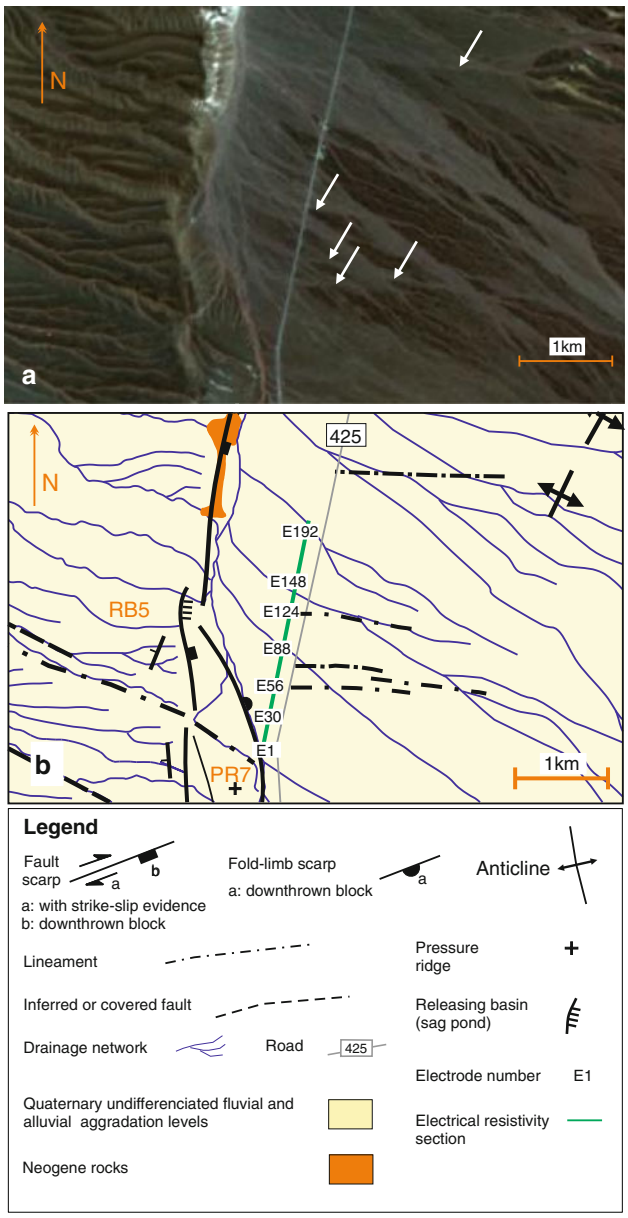

Fig. 10 The P7 survey cross-cuts oblique structures which are revealed (indicated by *arrows*) in the ASTER satellite image (RGB: 321, this figure) or aerial photographs. Locations of some electrodes are indicated as reference

Discussion

Subsurface structures of sections S3, S4 and S5 of the El Tigre Fault

The integration of previously presented data concerning the geometry of geomorphological features along the El Tigre Fault with the results of the ERTs allows to point out several observations regarding the subsurface structure of sections S3, S4 and S5 and their respective boundaries. The resistivity profiles P1 and P2, which revealed a subvertical and a high-angle east-dipping main fault plane, respectively, and observations reported from palaeoseismological trenches T2 (Siame 1998) and T3 (INPRES 1982), confirm that the S5 section of the fault has a normal component of displacement. This is consistent with the occurrence of a large releasing bend, consequence of a dextral strike-slip motion along a major right bend. The northern boundary of S5 is probably constituted by a major mechanical discontinuity, superficially expressed through a major lineament that crosses the El Tigre Fault (Fig. 2). The presence of significant folding of the Miocene sediments along S6 section contrasts significantly with the lack of such deformation in section S5. The presence of a large pressure ridge (PR8) at the southern tip of S6 is consistent with such interpretation as well as the 13° strike variation of the fault at such boundary and the different orientation of the trend of oblique transversal structures and lineaments from S6 (where they trend NW) in contrast to S5 and further south (where they trend WNW).

In the S4 section, the two profiles P3 and P4 allow to infer that the internal structure of the pressure ridges is controlled to the east by a high-angle reverse west-dipping fault with no evidence of an antithetic fault to depict a positive flower structure. In contrast, these gentle anticline structures developed for accommodating a component of compressive deformation along the main fault. This setting clearly corroborates a section dominated by a transpressive regime, as a consequence of the major left bend.

In the S3 section, the resistivity model P5 images a complex zone, although a subvertical fault could be inferred under a scarp. The P6 ERT shows a uniform pressure ridge controlled by a west-dipping fault on its eastern flank, supporting a reverse component of displacement. In this way, this section presents a complex or heterogeneous behaviour. The three pressure ridges (PR3, PR5 and PR7) that were imaged, in sections S4 and S3, through the ERTs, showed a similar pattern with a reverse fault on the eastern flank, and no evidence of a positive flower-type pattern as proposed by Bastías and Uliarte (1991). Another important consideration is that at least four out of the six resistivity profiles transversal to the El Tigre Fault (P1, P2, P3, P6) show that the sediments on the east (down-thrown) block of the fault have been significantly tilted towards the east against their depositional slope, at least up to a few hundred metres to the side of the fault. The systematic disturbance that the main fault shows in the low resistivity levels associated with the water table permits to consider the El Tigre Fault as an important hydrogeological barrier. In general, it has been observed that in this region the water table is probably located between 20 and 40 m deep.

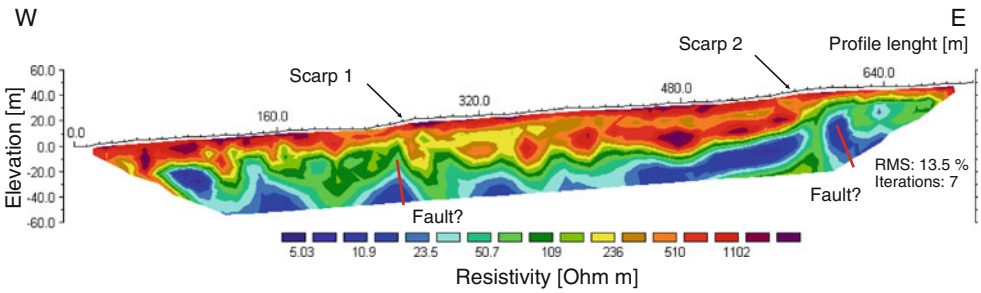

Fig. 11 P8 resistivity model carried out across minor structures on the western piedmont slope of the Sierra del Tigre (*array*: dipole–dipole; roll-along method; minimum unit electrode spacing: 10 m; smooth inversion; maximum penetration depth: 51 m)

Integration of structural and geomorphological studies with ERTs

Many proposals have been presented with reference to the deep geometry of the El Tigre Fault. Bastías et al. (1984) considered it a normal oblique-slip fault belonging to a much bigger fault system (named also the El Tigre Fault system). Later, Cardó and Díaz (2005) also regarded the fault as belonging to a major system, but as part of an east-verging thrust system with less than 9 km of depth. However, the hypothesis of normal faulting is in contrast with the cases of high-angle reverse faulting imaged by the ERTs here presented (i.e. P3, P4 and P6 surveys). This is also in contrast with the regional kinematics (Siame et al. 2006) and with the relative convergence direction of tectonic plates in this sector of the South American continental margin during the Quaternary (DeMets et al. 1990). Nevertheless, high-angle normal faulting was also revealed by the ERT (P2 survey) confirming observations made at palaeoseismological trenches (Siame 1998).

The remarkable linear fault trace that is observed in satellite imagery and aerial photographs (especially in the Central and Southern Segments) is consistent with a subvertical geometry at depth which is in agreement with the fault model proposed by Siame et al. (1997b). Furthermore, the geomorphological observations and geophysical results in the Central Segment are compatible with a high-angle fault with irregularities consisting in major right or left bends which define sections of transtensive or transpressive character, respectively, so that the fault dip adjusts to a local tectonic regime occurring at hectometric to kilometric scale. These local variations are expressed as sections of a few kilometres in length with relatively homogeneous behaviour and frequently separated by oblique or transversal structures. These local changes are also expressed in abrupt changes in the fault trace trend that may be of more than 10°. Whether these boundaries are controlled by major, likely inherited, structures and their deep geometry and kinematics await further investigations.

Conclusions

The strike-slip El Tigre Fault, in the Central–Western Precordillera of San Juan Province, Argentina, represents a significant object of neotectonic interest due to its remarkable extension, clear geomorphic expression, Quaternary activity and location in a major seismically active region. The integration of the geophysical and geological approaches provided original and important information about the geomorphology, the structure and the geometry at shallow depth of this outstanding fault. Among the observations made, we identified (in the Central and Southern Segments of the El Tigre Fault) geometric discontinuities (left and right bends, stepovers) and structural discontinuities (splays, intersection of the main fault trace with other structures), all of them having an inhomogeneous distribution along the fault trace. In addition, it was possible to recognize several pressure ridges and sag ponds corresponding to minor restraining and releasing bends, respectively, associated with the right-lateral strike-slip displacement. The presence of several fault strands differentiated by relative changes in their strike and the concentration of specific geomorphological features within those strands allowed to propose the definition of six major sections along the main fault in the Central and Southern Segments. Combining that information with the resistivity surveys carried out in the Central Segment, it is also suggested that some of these sections are associated with major restraining or releasing areas, respectively, as revealed by the west or east-dipping main fault plane as inferred by the ERTs. Accordingly, the global geometry of the Central Segment is consistent with an alternating high-angle west-dipping (reverse) or east-dipping (normal) fault in the different sections. This interpretation is in agreement with that proposed by Siame et al. (1997b) who considered that the El Tigre Fault has as subvertical geometry at depth. In this work, we also propose slight modifications to the fault segmentation suggested previously by Siame et al. (1997b).

Acknowledgments The authors are very grateful for the financial provided by Universidad de Buenos Aires (UBACyT

20020100100778 and UBACyT 100597 grants) and CONICET (PIP-CONICET 11220080102295 grant). We also would like to thank Horacio Lippai for technical support. ASTER satellite imagery was kindly provided by SEGEMAR. Daniel Pérez generously contributed in their preparation. Careful corrections and suggestions from Riccardo Caputo and Jonas Kley, which helped to improve the manuscript, are deeply appreciated and thanked.

References

Abad ME, Robles A, Manrique W, Bastías H (1990) Control de movimientos tectónicos en la falla "El Tigre". 11° Congreso Geológico Argentino. San Juan. Actas 2:449–451

Allmendinger RW, Figueroa D, Snyder D, Beer J, Mpodozis C, Isacks BL (1990) Foreland shortening and crustal balancing in the Andes at 30°S latitude. Tectonics 9:789–809

Aparicio EP (1984) Geología de San Juan. Facultad de Ciencias exactas, Físicas y Naturales, Universidad Nacional de San Juan, San Juan, 167 pp

Baldis BA, Beresi MS, Bordonaro LO, Vaca A (1982) Síntesis evolutiva de la Precordillera Argentina. 5º Congreso Latinoamericano de Geología, Buenos Aires. Actas 4:399–445

Baraldo JA, Montea AL, Soechting W (1990) Triásico de San Juan. In: Bordonaro O (ed) Relatorio de Geología y Recursos Naturales de la provincia de San Juan, 124–139. 11° Congreso Geológico Argentino, San Juan

Basile YA (2004) Estudio geológico y geofísico del sector sur de las Lomas del Inca, provincia de San Juan. Trabajo final de Licenciatura. Facultad de Ciencias Exactas y Naturales, Universidad de Buenos Aires, 125 pp

Bastías HE (1985) Fallamiento cuaternario en la región sismotectónica de Precordillera. Tesis Doctoral. Facultad de Ciencias Exactas, Físicas y Naturales, Universidad Nacional de San Juan, 160 pp

Bastías J (1989) Morfología y análisis de desplazamiento en la falla El Tigre-San Juan, Argentina. Tesis de licenciatura. Facultad de Ciencias Exactas, Físicas y Naturales, Universidad Nacional de San Juan, 95 pp

Bastías HE (1990a) Discontinuidades tectónicas a la latitud de 32° Sur y su importancia en las hipótesis de evolución de Precordillera. 11° Congreso Geológico Argentino, San Juan. Actas 2:407–411

Bastías JA (1990b) Noroeste argentino-Fallas transcurrentes. Cuencas transtensivas. 11° Congreso Geológico Argentino, San Juan. Actas 2:413–416

Bastías HE, Bastías JA (1987) Fallamiento rumbo-deslizante en el borde oriental de los Andes entre los 32 y 26 grados de latitud sur. 10° Congreso Geológico Argentino, San Miguel de Tucumán. Actas 1:207–210

Bastías HE, Uliarte E (1987) Morfología de la falla rumbo—deslizante El Tigre entre los ríos Jáchal y San Juan. 10° Congreso Geológico Argentino, San Miguel de Tucumán. Actas 1:251–254

Bastías JA, Uliarte E (1991) Tectoformas de transcurrencias, Falla El Tigre, sector central, San Juan, Argentina. 6° Congreso Geológico Chileno. Volumen 1. Resúmenes expandidos, 505–509

Bastías HE, Weidmann NE, Pérez AM (1984) Dos zonas de fallamiento Pliocuaternario en la Precordillera de San Juan. 9° Congreso Geológico Argentino, S.C. Bariloche. Actas 2:329–341

Bastías H, Uliarte E, Pérez MA (1985) Desplazamiento de rumbo en el sistema de fallamiento El Tigre, borde occidental de Precordillera. Primeras Jornadas Geológicas de Precordillera. San Juan. Actas 1:221–225

Bastías HE, Uliarte E Paredes J de D, Sanchez A, Bastías JA, Ruzycki L, Perucca P (1990) Neotectónica de la provincia de San Juan. 11° Congreso Geológico Argentino, San Juan. Relatorio de geología y recursos naturales de la Provincia de San Juan, pp 228–244

Bastías HE, Tello GE, Perucca LP, Paredes J de D (1993) Peligro sísmico y neotectónica. 12° Congreso Geológico Argentino y 2° Congreso de Exploración de Hidrocarburos (Mendoza), In: Ramos VA (ed) Geología y Recursos Naturales de Mendoza. Relatorio 6(1):645–658

Beer JA, Allmendinger RW, Figueroa DA, Jordan TE (1990) Seismic stratigraphy of a Neogene piggy-back basin, Argentina. Am Assoc Petr Geol Bull 74:1183–1202

Caputo R, Piscitelli S, Oliveto A, Rizzo E, Lapenna V (2003) The use of electrical resistivity tomographies in active tectonics: examples from Tyrnavos Basin, Greece. J Geodyn 36:19–35

Caputo R, Salviulo L, Piscitelli S, Loperte A (2007) Late Quaternary activity along the Scorciabuoi Fault (Southern Italy) as inferred from electrical resistivity tomographies. Ann Geophys 50(2):213–223

Cardó R, Díaz IN (2005) Memoria Hoja Geológica 3169-I, Rodeo. Servicio Geológico Minero Argentino, Buenos Aires

Colella A, Lapenna V, Rizzo E (2004) High-resolution imaging of the High Agri Valley Basin (Southern Italy) with electrical resistivity tomography. Tectonophysics 386:29–40

Contreras VH, Damiani O, Milana JP, Bracco AI, Barrera OM (1990) Paleógeno y Neógeno de San Juan. 11° Congreso Geológico Argentino, San Juan. Actas, pp 154–185

Cortés JM, Cegarra M (2004) Plegamiento cuaternario transpresivo en el piedemonte suroccidental de la Precordillera sanjuanina. Asociación Geológica Argentina, Serie D, Publicación Especial N°7, pp 68–75, Buenos Aires

Cortés JM, Vinciguerra P, Yamín M, Pasini MM (1999) Tectónica Cuaternaria de la Región Andina del Nuevo Cuyo (28°–38° LS). In: Caminos R (ed): Geología Argentina. Subsecretaría de Minería de la Nación, Servicio Geológico Minero Argentino, Anales 29, Cap. 24, pp 760–778, Buenos Aires

Cortés JM, Pasini, MM, Yamín G (2005a) Paleotectonic controls on the distribution of Quaternary deformation in Southern Precordillera, Central Andes (31°30′–33°SL). International Symposium on Andean Geodynamics, extended abstracts, pp 186–189, Barcelona

Cortés JM, Yamín MG, Pasini MM (2005b) La Precordillera Sur, Provincias de Mendoza y San Juan. 16° Congreso Geológico Argentino, La Plata. Actas 1:395–402

Cortés JM, Casa A, Pasini MM, Yamín MG (2005c) Fajas de estructuras neotectónicas asociadas a rasgos paleotectónicos en Precordillera y Cordillera Frontal (31°30′–33°30′LS). 16° Congreso Geológico Argentino, La Plata. Actas 4:463–466

Cortés JM, Casa A, Pasini MM, Yamín MG, Terrizzano CM (2006) Fajas oblicuas de deformación neotectónica en Precordillera y Cordillera Frontal (31°30′–33°30′LS). Controles paleotectónicos. Revista de la Asociación Geológica Argentina 61(4):639–646

Costa C, Machette MN, Dart RL, Bastías E, Paredes ND, Perucca LP, Tello GE, Haller KM (2000) Map and database of Quaternary Faults and Folds in Argentina. United States geological survey open-file reports 00-108, 75 pp

Costa CH, Audemard MFA, Bezerra FHR, Lavenu A, Machette MN, París G (2006) An overview of the main quaternary deformation of South America. Revista de la Asociación Geológica Argentina 61(4):461–479

Crone AJ, Heller KM (1991) Segmentation and the coseismic behaviour of Basin and Range normal faults: examples from

east-central Idaho and southwestern Montana. USA J Struct Geol 13:151–164

Demanet D, Pirard E, Renardy F, Jongmans D (2001a) Application and processing of geophysical images for mapping faults. Comput Geosci 27:1031–1037

Demanet D, Renardy F, Vanneste K, Jongmas D, Camelbeek T, Megharaoui M (2001b) The use of geophysical prospecting for imaging active faults in the Roer Graben, Belgium. Geophysics 66(1):78–89

DeMets C, Gordon RG, Argus DF, Stein S (1990) Current plate motions. Geophys J Int 101:425–478

Donne DD, Piccardi L, Odum JK, Stephenson WJ, Williams RA (2007) High-resolution shallow reflection seismic image and surface evidence of the Upper Tiber Basin active faults (Northern Apennines, Italy). B Soc Geol Ital 126(3):326–331

Esper Angillieri MY (2007) El aluvión del 13 de febrero de 1944 en la quebrada del Carrizal, departamento Iglesia, provincia de San Juan. Revista de la Asociación Geológica Argentina 62(2):283–288

Fazzito SY (2011) Estudios geofísicos aplicados a la neotectónica de la falla El Tigre, Precordillera de San Juan. Tesis doctoral. Facultad de Ciencias Exactas y Naturales, Universidad de Buenos Aires, 260 pp

Fazzito SY, Rapalini AE, Cortés JM (2006) Tomografía geoeléctrica en zonas de falla cuaternarias: dos ejemplos en la Precordillera centro-occidental de Mendoza. Revista de la Asociación Geológica Argentina, Serie D, Publicación especial N° 9: 41–47

Fazzito SY, Rapalini AE, Cortés JM, Terrizzano CM (2009) Characterization of Quaternary faults by electric resistivity tomography in the Andean Precordillera of Western Argentina. J S Am Earth Sci 28:217–228

Fernandez AE (1995) Seismic analysis, paleoclimatology and fluvial architecture of the Bermejo basin, Central Andes, Western Argentina. A dissertation presented to the Faculty of the Graduate School of Cornell University in Partial Fulfilment of the requirements for the Degree of Doctor of Philosophy, 279 pp

Fleta J, Santanach P, Martinez P, Goula X, Grellet B, Masana E (2000) Geologic, geomorphologic and geophysic approaches for the paleoseismological analysis of the Amer fault (NE Spain). Workshop Proceedings of HAN2000: Evaluation of the potential for large earthquakes in regions of present day low seismic activity in Europe, Han-sur-Lesse, Belgium, pp 63–66

Furque G (1963) Descripción Geológica de la Hoja 17b-Guandacol. Servicio Geológico Nacional, Boletín 92, Buenos Aires, 104 pp

Gagliardo M, Caselli A, Limarino O, Colombo Piñol F, Tripaldi A (2001) Las unidades terciarias de la Cuenca Rodeo-Iglesia: validez y correlación de las unidades formacionales. Revista de la Asociación Geológica Argentina 56(1):121–125

Giano SI, Lapenna V, Piscitelli S, Schiattarella M (2000) Electrical imaging and self-potential surveys to study the geological setting of the Quaternary slope deposits in the Agri high valley (Southern Italy), 2000. Ann Geofis 43(2):409–419

Hanks T, Kanamori H (1979) A moment magnitude scale. J Geophys Res 84 (B5):2348–2350

INPRES (1977) Zonificación sísmica de la República Argentina. Instituto Nacional de Prevención Sísmica, Publicación Técnica n° 5, San Juan, 41 pp

INPRES (1982) Microzonificación sísmica del valle de Tulúm, provincia de San Juan. Instituto Nacional de Prevención Sísmica. Resumen Ejecutivo, San Juan

Isacks B, Barazangi M (1977) Geometry of Benioff zones: lateral segmentation and downwards bending of the subducted lithosphere. In: Talwani M, Pitman W (eds), Island Arcs, Deep Sea Trenches and Back Arc Basins American Geophysical Union, Ewing Series 1, pp 99–114

Johnson AT, Jordan TE, Johnson NM, Naeser C (1987) Cronología y velocidad de sedimentación en una secuencia volcaniclástica, Rodeo, Prov. de San Juan, Rep. Argentina. 10° Congreso Geológico Argentino, Tucumán. Actas 2:87–90

Jordan TE, Isacks BL, Allmendinger RW, Brewer JA, Ramos VA, Ando CJ (1983a) Andean tectonics related to geometry of subducted Nazca plate. Geol Soc Am Bull 94(3):341–361

Jordan TE, Isacks B, Ramos VA, Allmendinger RW (1983b) Mountain building in the Central Andes. Episodes 3:20–26

Jordan TE, Allmendinger RW, Damanti JF, Drake R (1993) Chronology of motion in a complete thrust belt: the Precordillera, 30–31°S, Andes Mountains. J Geol 101:135–156

Jordan T, Kelley S, Fernández A, Fernández Seveso F, Re G, Milana JP (1997) Relaciones entre las historias evolutivas de las cuencas de Iglesia y Bermejo, provincia de San Juan, Argentina. 2° Jornadas sobre Geología de Precordillera, San Juan. Actas 1:142–147

Kay SM, Abbruzzi JM (1996) Magmatic evidence for Neogene lithospheric evolution of the Central Andean flat-slab between 30 and 32°S. Tectonophysics 259:15–28

Leveratto MA (1976) Edad de intrusitos cenozoicos en la Precordillera de San Juan y su implicancia estratigráfica. Revista de la Asociación geológica Argentina 31(1):53–58

Loke MH (1996–2011) Tutorial: 2-D and 3-D electrical imaging surveys. Geotomo Software

Loke MH (2001) Rapid 2-D resistivity and IP inversion using the least-squares method. Geoelectrical Imaging 2-D and 3-D. Geotomo Software

Mann P, Hempton MR, Bradley DC, Burke K (1983) Development of pull-apart basins. J Geol 91(5):529–554

Nguyen F, Garambois S, Jongmans D, Pirard E, Loke MH (2005) Image processing of 2D resistivity data for imaging faults. J Appl Geophys 57(4):260–277

Nguyen F, Garambois S, Chardon D, Hermitte D, Bellier O, Jongmans D (2007) Subsurface electrical imaging of anisotropic formations affected by a slow active reverse fault, Provence, France. J Appl Geophys 62(4):338–353

Nivière B, Bruestle A, Bertrand G, Carretier S, Behrmann J, Gourry JC (2008) Active tectonics of the southeastern Upper Rhine Graben, Freiburg area (Germany). Quat Sci Rev 27:541–555

Ortiz A, Zambrano JJ (1981) La provincia geológica Precordillera Oriental. 8° Congreso Geológico Argentino, San Luis. Actas 3:59–74

Pánek T, Tábořík P, Klimeš J, Komárková V, Hradecký J, Šťastný M (2011) Deep-seated gravitational slope deformations in the highest parts of the Czech Flysch Carpathians: evolutionary model based on kinematic analysis, electrical imaging and trenching. Geomorphology 129(1–2):92–112

Paredes JdeD (1990) Pampa del Jarillal, una cuenca trastensiva en la Precordillera de San Juan, Argentina. 11° Congreso Geológico Argentino, San Juan. Actas 2:427–429

Pérez I, Costa C (2006). El sistema de fallamiento EL Tigre entre el río Jáchal y el cerro Negro de Iglesia (provincia de San Juan). 13° Reunión de Tectónica, San Luis. Abstracts 80

Ramos VA, Cristallini EO, Pérez DJ (2002) The Pampean flat-slab of the Central Andes. J S Am Earth Sci 15(1):59–78

Re G (1994) Magnetoestratigrafía de la secuencia neogénica aflorante en arroyo Chaleta (Angualasto, San Juan), sus implicancias tectosedimentarias. 5° Jornadas Argentinas de Sedimentología, Tucumán. Abstracts, pp 205–209

Re G, Barredo S (1993) Estudio magnetoestratigráfico y tasa de sedimentación del Grupo Iglesia en sus afloramientos aledaños a la localidad de Angualasto (Prov. de San Juan). 12° Congreso Geológico Argentino. Actas 2:148–155

Re GH, Jordan TE, Kelley S (2003) Cronología y paleogeografía del Terciario de la Cuenca Intermontana de Iglesia septentrional, Andes de San Juan, Argentina. Revista de la Asociación Geológica Argent 58(1):31–48

Rizzo E, Colella A, Lapenna V, Piscitelli S (2004) High-resolution images of the fault-controlled High Agri Valley basin (Southern Italy) with deep and shallow electrical resistivity tomographies. Phys Chem Earth 29:321–327

Siame LL (1998) Cosmonucléide produit in situ (10Be) et quantification de la déformation active dans les Andes centrales. Thèse de doctorat. Université de Paris-Sud, Orsay

Siame LL, Sébrier M, Bellier O, Bourles DL, Castano JC, Araujo M, Yiou F, Raisbeck GM (1996) Segmentation and horizontal slip-rate estimation of the El Tigre Fault Zone, San Juan Province (Argentina) from SPOT images analysis. Third ISAG (St Malo, France), pp 239–241

Siame LL, Bourles DL, Sébrier M, Bellier O, Castano JC, Araujo M, Perez M, Raisbeck GM, Yiou F (1997a) Cosmogenic dating ranging from 20 to 700 ka of a series of alluvial fan surfaces affected by the El Tigre Fault, Argentina. Geology 25(11):975–978

Siame LL, Sébrier M, Bellier O, Bourlès DL, Castano JC, Araujo M (1997b) Geometry, segmentation and displacement rates of the El Tigre Fault, San Juan Province (Argentina) from SPOT image analysis and ^{10}Be datings. Annales Tectonicae 1(2):3–26

Siame LL, Bellier O, Sebrier M (2006) Active tectonics in the Argentine Precordillera and western Sierras Pampeanas. Revista de la Asociación Geológica Argent 61(4):604–619

Stewart IS, Hancock PL (1991) Scales of structural heterogeneity within neotectonic fault zones in the Aegean region. J Struct Geol 13:191–204

Storz H, Storz W, Jacobs F (2000) Electrical resistivity tomography to investigate geological structures of the earth's upper crust. Geophys Prospect 48:455–471

Suzuki K, Toda S, Kusunoki K, Fujimitsu Y, Mogi T, Jomori A (2000) Case studies of electrical and electromagnetic methods applied to mapping active faults beneath the thick quaternary. Eng Geol 56:29–45

Telford WM, Geldart LP, Sheriff RE (1990) Applied geophysics, 2nd edn. Cambridge University Press, Cambridge

Terrizzano CM (2010) Neotectónica del extremo noroccidental del cinturón Barreal—Las Peñas, Precordillera Sur. Tesis doctoral. Facultad de Ciencias Exactas y Naturales, Universidad de Buenos Aires, 292 pp

Terrizzano CM, Cortés JM, Fazzito SY, Rapalini AE (2008) Neotectonic transpressive zones in Precordillera Sur, Central Andes of Argentina: a structural and geophysical investigation. Neues Jahrb Geol P-A 253(1):103–114

Terrizzano CM, Fazzito SY, Cortés JM, Rapalini AE (2010) Studies of Quaternary deformation zones through geomorphic and geophysical evidence: a case in the Precordillera Sur. Central Andes of Argentina. Tectonophysics 490(3–4):184–194

Terrizzano CM, Fazzito SY, Cortés JM, Rapalini AE (2012) Electrical resistivity tomography applied to the study of neotectonic structures, northwestern Precordillera Sur, Central Andes of Argentina. J S Am Earth Sci 34:47–60

Vallejo MD (2004) Estudio geológico y geofísico del sector norte de Lomas del Inca, Barreal del Leoncito, San Juan. Trabajo final de Licenciatura. Facultad de Ciencias Exactas y Naturales, Universidad de Buenos Aires

Verbeeck K, Beatse H, Vanneste K, Renardy F, Van Der Meer H, Roy-Chowdhury K, Camelbeeck T (2000) Geomorphic and geophysical reconnaissance of the Reppel and Bocholt faults, NE Belgium. Workshop proceedings of HAN2000: Evaluation of the potential for large earthquakes in regions of present day low seismic activity in Europe", Han-sur-Lesse, Belgium, pp 167–170

von Gosen W (1995) Polyphase structural evolution of the southwestern Argentine Precordillera. J S Am Earth Sci 8(3–4):377–404

Wang CY (2002) Detection of a recent earthquake fault by the shallow reflection seismic method. Geophysics 67(5):1465–1473

Weidmann R, Cardinal A, Simon W (1985) Propuesta de ordenamiento de la nomenclatura estratigráfica de las sedimentitas terciarias de la Precordillera sanjuanina. Primeras Jornadas sobre geología de Precordillera, San Juan, pp 342–347

Wetten C (1975a) Geología del valle de Iglesia, su relación con los yacimientos de diatomita de Lomas del Campanario e importancia económica. Trabajo Final de Licenciatura. Facultad de Ciencias Exactas, Físicas y Naturales, Universidad Nacional de San Juan, 70 pp

Wetten C (1975b) Estudio geológico económico de un yacimiento de diatomita y análisis de mercado. 2° Congreso Iberoamericano de Geología Económica. Actas 5:513–529

Whitney RA (1990) Trenching of active faults in the San Juan Province of west-Central, Argentina. 11° Congreso Geológico Argentino, San Juan. Actas 2:445–446

Wise DJ, Cassidy J, Locke CA (2003) Geophysical imaging of the Quaternary Wairoa North Fault, New Zealand: a case study. J Appl Geophys 53:1–16

Woodcock NH, Fischer M (1986) Strike-slip duplexes. J Struct Geol 25:725–735

Woodcock NH, Schubert C (1994) Continental strike-slip tectonics. In: Hancock PL (ed) Continental deformation. Pergamon Press, Oxford, pp 251–263

Yamín MG (2007) Neotectónica del bloque Barreal, margen noroccidental de la Precordillera Sur. Tesis doctoral. Facultad de Ciencias Exactas y Naturales, Universidad de Buenos Aires

Zapata TR, Allmendinger RW (1996) Thrust-front zone of the Precordillera, Argentina: a thick-skinned triangle zone. Am Assoc Petr Geol Bull 80:359–381